

Active cooling of microvascular composites for battery packaging

This content has been downloaded from IOPscience. Please scroll down to see the full text.

2017 Smart Mater. Struct. 26 105004

(<http://iopscience.iop.org/0964-1726/26/10/105004>)

View [the table of contents for this issue](#), or go to the [journal homepage](#) for more

Download details:

IP Address: 128.174.44.54

This content was downloaded on 02/09/2017 at 16:22

Please note that [terms and conditions apply](#).

You may also be interested in:

[Numerical simulations for microvascular shape memory polymer composites](#)

Y Li and N C Goulbourne

[On-chip thermal management of hotspots using a perspiration nanopatch](#)

Shankar Narayanan, Andrei G Fedorov and Yogendra K Joshi

[Hierarchical system for autonomous sensing-healing of delamination in large-scale composite structures](#)

Shu Minakuchi, Denghao Sun and Nobuo Takeda

[Evaluation and modelling of two urethral cooling catheters](#)

Sean R H Davidson and Michael D Sherar

[Design optimization of a microfluidic-integrated thermoelectric power generator](#)

Yeh En Heng, Asrulnizam Abd Manaf and Sze Sing Lee

[Experimental and theoretical analysis of a hybrid solar thermoelectric generator with forced convection cooling](#)

Pradeepkumar Sundarraj, Robert A Taylor, Debosmita Banerjee et al.

[Numerical simulation of phase images and depth reconstruction in pulsed phase thermography](#)

Saul Hernandez-Valle and Kara Peters

[Hydraulic and thermal design of a gas microchannel heat exchanger](#)

Yahui Yang, Juergen J Brandner and Gian Luca Morini

Active cooling of microvascular composites for battery packaging

Stephen J Pety^{1,3}, Patrick X L Chia^{2,3}, Stephen M Carrington^{2,3} and Scott R White^{2,3}

¹Department of Materials Science and Engineering, University of Illinois at Urbana-Champaign, 1304 W Green St., Urbana, IL 61801, United States of America

²Department of Aerospace Engineering, University of Illinois at Urbana-Champaign, 104 S. Wright St., Urbana, IL 61801, United States of America

³Beckman Institute for Advanced Science and Technology, University of Illinois at Urbana-Champaign, 405 N Mathews Av., Urbana, IL 61801, United States of America

E-mail: swhite@illinois.edu

Received 13 April 2017, revised 31 July 2017

Accepted for publication 8 August 2017

Published 1 September 2017



CrossMark

Abstract

Batteries in electric vehicles (EVs) require a packaging system that provides both thermal regulation and crash protection. A novel packaging scheme is presented that uses active cooling of microvascular carbon fiber reinforced composites to accomplish this multifunctional objective. Microvascular carbon fiber/epoxy composite panels were fabricated and their cooling performance assessed over a range of thermal loads and experimental conditions. Tests were performed for different values of coolant flow rate, channel spacing, panel thermal conductivity, and applied heat flux. More efficient cooling occurs when the coolant flow rate is increased, channel spacing is reduced, and thermal conductivity of the host composite is increased. Computational fluid dynamics (CFD) simulations were also performed and correlate well with the experimental data. CFD simulations of a typical EV battery pack confirm that microvascular composite panels can adequately cool battery cells generating 500 W m^{-2} heat flux below 40°C .

Supplementary material for this article is available [online](#)

Keywords: microvascular composites, battery cooling, computational fluid dynamics, thermal imaging, multifunctional materials

(Some figures may appear in colour only in the online journal)

1. Introduction

A key challenge for high-range electric vehicles (EVs) is packaging the large number of battery cells required. Battery packaging must simultaneously maintain an optimal temperature for battery operation while also protecting batteries in the event of a crash.

It is critical that temperature is regulated for the lithium-ion batteries used in most EVs, since operating temperatures outside of the range 10°C – 40°C lead to poor cycling performance and reduced lifetime [1, 2]. Prismatic batteries produce in the range of 1–30 W of waste heat during deep cycling, with the highest heat generation occurring at high discharge rate and high degree of discharge [3]. Batteries are

also subject to heating and cooling from operation in warm or cold climates [4]. Finally, cell damage can lead to sudden increases in temperature that can potentially lead to thermal runaway and fire [5]. In order to maintain optimal performance and protect batteries from thermal runaway, most EVs employ an active thermal management system using either air [6] or a liquid coolant [7–9]. Alternate cooling schemes have also been proposed using heat pipes [10] or phase change materials [11].

Battery packaging must also protect batteries during crashes. This has led to complex packaging such as the scheme used for the Chevy Volt, where liquid coolant circulates through aluminum cooling panels sandwiching the battery cells while an outer casing of fiberglass and steel

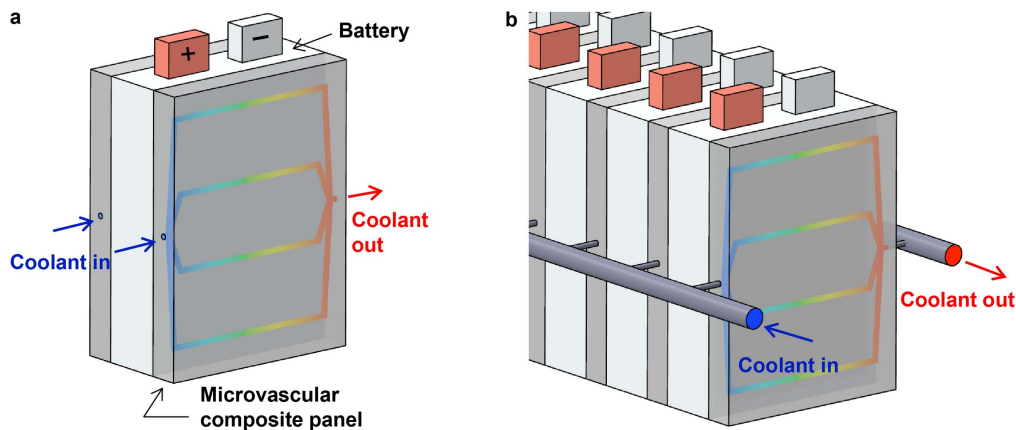


Figure 1. Schematic of battery packaging using microvascular composite panels. (a) A battery cell is sandwiched between two microvascular composite panels through which coolant flows. (b) Assembly of multiple battery cells with a coolant distribution manifold.

protects the cells during a crash [7, 8]. Despite such complex and heavy protection schemes, several EV battery packs have caught on fire after crashes in recent years due to damaged batteries and cooling systems [12, 13]. A need exists for an integrated, lightweight packaging system that can provide superior structural protection with simultaneous thermal management. Fiber-reinforced composites are one potential materials system with superior crashworthiness. Carbon/epoxy fiber-reinforced composites fail in a crash through a combination of compressive failure and splaying (delamination and bending) which leads to material disintegration [14]. The specific energy absorbed (SEA) ranges from 50–100 kJ kg⁻¹ [15]. For comparison, typical SEA values are ca. 30 kJ kg⁻¹ for aluminum and ca. 20 kJ kg⁻¹ for steel [15]. Composite battery packaging can thus provide significantly increased crashworthiness compared to metals while also reducing weight. Reduced weight in turn leads to extended range, as realized in EVs that utilize carbon/epoxy composites such as the BMW i3 [16].

Fiber-reinforced composites have also been used for the integration of microvascular channels for coolant flow [17–22]. The majority of studies to date have focused on cooling polymer matrix composites in high heat flux environments to keep them below their glass transition temperature (ca. 150 °C). Soghrati *et al* simulated cooling of a microvascular glass-fiber/epoxy composite subject to heat fluxes representative of hypersonic flight [18]. Composites with high coolant flow rate and channel density maintained temperatures below 150 °C at heat fluxes as high as 100 kW m⁻². Coppola *et al* measured the flexural modulus of microvascular glass-fiber/epoxy composites at elevated ambient temperatures [19] and demonstrated up to 90% retention of modulus at an ambient temperature of 325 °C. Coppola *et al* also demonstrated the retention of compressive strength for vascular carbon fiber/epoxy composites subject to heat fluxes as high as 60 kW m⁻² [21]. As an alternate application, microchannels have also been used to actuate shape memory composites through the flow of heated fluids [23, 24].

While these prior studies demonstrated the utility of actively cooled/heated composites, none have considered the use of composites as cooling panels designed to keep a heat

source (e.g. a battery) within a narrow temperature range. Prior studies have focused on composite panels with relatively small planar area (<100 mm × 100 mm) compared to EV batteries. Finally, while some studies showed agreement between experiment and simulation, their scope has been restricted to a limited number of test conditions.

Here we propose a novel battery packaging scheme where a single material provides both cooling and crash protection. Batteries are embedded within microvascular carbon fiber/epoxy composites through which coolant can flow (figure 1(a)). Batteries can be stacked into a single pack (figure 1(b)), with additional composite reinforcement seamlessly added around the pack exterior as needed. Alternatively, batteries can be embedded within composite body panels to achieve system-level savings of volume and weight [25, 26]. With either packaging scheme, batteries are protected by composites that have a higher specific strength, stiffness, and crashworthiness than aluminum or steel [27, 28].

The cooling performance of microvascular composite cooling panels is characterized using both experiments and simulations. Microvascular composites are fabricated by vacuum-assisted resin transfer molding (VARTM) and the use of sacrificial fibers. Cooling performance is characterized across a range of coolant flow rates, applied heat fluxes, channel spacings, and carbon fiber materials. Computational fluid dynamics (CFD) simulations are also performed and are validated across all experimental test conditions. Finally, further simulations are performed to design vascular cooling panels for use in a typical EV battery pack. Simulations are performed using different panel materials, channel spacings, applied heat fluxes, coolant flow rates, and panel thicknesses. A detailed crashworthiness study of microvascular carbon/epoxy composites is presented in a separate work [29].

2. Methods

2.1. Fabrication of microvascular composite panels

Microvascular composite panels were prepared using VARTM. Panels were made with both polyacrylonitrile

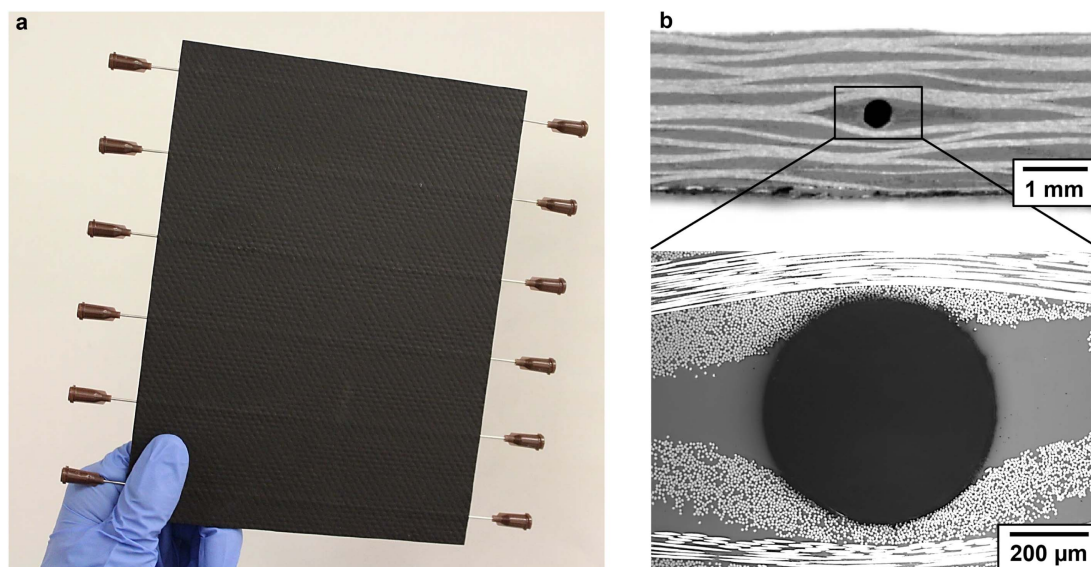


Figure 2. Microvascular composite panel. (a) 150 mm \times 200 mm carbon fiber/epoxy panel with 6 cooling channels (500 μ m diameter) with inlet and outlet needles attached. (b) Cross-sectional optical micrographs of a 500 μ m diameter cooling channel embedded in a carbon/epoxy composite.

(PAN) and pitch derived carbon fiber fabrics. The PAN-based fabric used was a 2 \times 2 twill weave of Toray T300 3 K fiber (199 g m⁻², Soller Composites) and the pitch-based fabric was a plain weave of ThermalGraph EWC-300X 4 K fiber (610 g m⁻², Cytec). Fabrics were infused with an epoxy resin composed of 100:35 Araldite LY 8605 epoxide to Aradur 8605 curing agent (Huntsman Advanced Materials, LLC).

For PAN-based carbon/epoxy panels, 12 layers of carbon fiber fabric were stacked in a double vacuum bag layup with 500 μ m diameter sacrificial fibers placed between the 6th and 7th layers of fabric (figure S1 is available online at stacks.iop.org/SMS/26/105004/mmedia). Channels were evenly spaced throughout the panel (see table S1 for channel spacings for different panels). For all panels but one, the sacrificial fibers were nylon monofilament (Berkley) treated with Henkel FREKOTE release agent (Northern Composites) and were manually extracted after cure. As a proof of concept, in one panel polylactide (PLA) fibers treated with tin (II) oxalate catalyst were used as sacrificial fibers and removed using the VaSC technique [30]. The sacrificial PLA fibers were prepared using a modified solvent-impregnation procedure adapted from Esser-Kahn *et al* [30] and Dong *et al* [31] (see section S1 for details).

Prior to infusion, epoxy resin was mixed by hand and degassed for 3 h at room temperature. Resin was infused into the fabric layup using a vacuum pump at \sim 38 Torr. The resin was cured at room temperature under vacuum for 24 h and then 121 $^{\circ}$ C for 2 h followed by 177 $^{\circ}$ C for 3 h. The heating rate was 2 $^{\circ}$ C min⁻¹ and the cooling rate to ambient was 1 $^{\circ}$ C min⁻¹. The average thickness of the PAN-based carbon/epoxy panels was 2.71 \pm 0.07 mm which corresponds to a fiber volume fraction of 49.5 \pm 1.3% based on ASTM D3171 (Test Method II).

After cure, the sacrificial nylon fibers were manually extracted using needle-nose pliers. This technique produced high-fidelity circular channels with little disruption to fiber architecture (figure 2). PLA fibers were evacuated through the VaSC process (200 $^{\circ}$ C and vacuum for 48 h) and gave similar quality channels. The VaSC process requires longer manufacturing time, but it is more scalable and can create channels with much more complex shapes [30, 32].

One pitch-based carbon/epoxy panel was made using 4 layers of carbon fiber fabric in a double vacuum bag layup with sacrificial fibers placed between the 2nd and 3rd layers of fabric. The pitch-based carbon/epoxy panel had a thickness of 3.03 mm which corresponds to a fiber volume fraction of 38.3%.

2.2. Cooling experiments

Vascular panels were cut to 150 mm \times 200 mm with a sectioning saw (Buehler IsoMet 1000) and the top surface was painted with a matte black paint (Krylon) for thermal imaging. Inlet and outlet holes 1.03 mm in diameter and 3 mm deep were drilled into each channel to allow the insertion of needle fittings. Cooling tests were performed using the experimental setup shown in figure 3(a). Panels were placed on top of a copper plate coupled to a polyimide flexible heater (Omega, part # KH-608/2) with thermal grease (Omega, part # Omegatherm 201). Applied heat flux was controlled by regulating the voltage supplied to the heater (see section S2) with a Variac variable transformer (Staco Energy Products Co., Type L1010). The heater assembly was placed on a balsa wood platform while the sides were insulated using fiberglass insulation.

The coolant was a 50:50 water/ethylene glycol mixture (Macron Chemicals) and was stored in a circulator (Julabo,

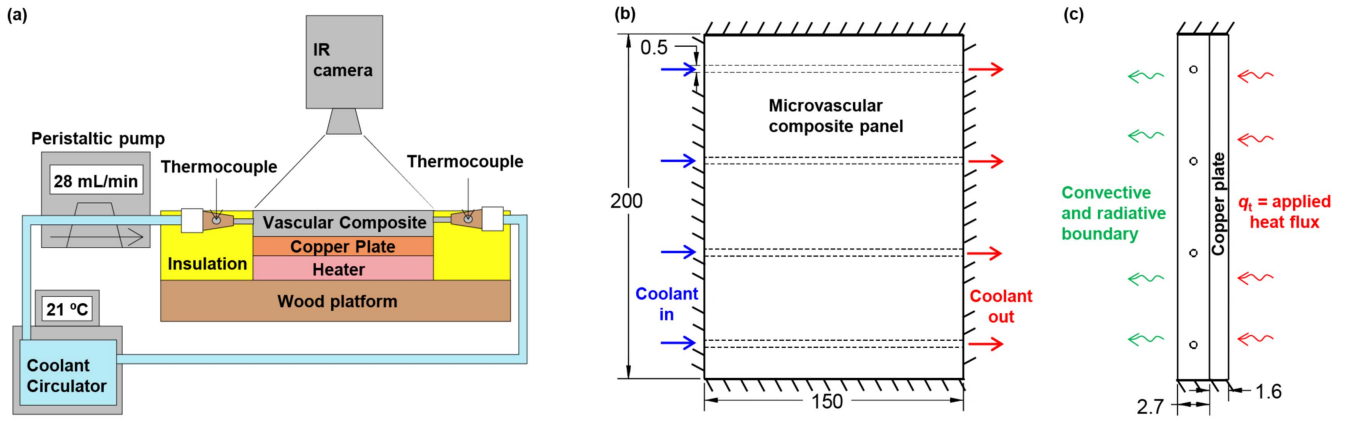


Figure 3. Schematics of cooling experiments and simulations. (a) Experimental setup where panel temperature is measured with an IR camera while coolant temperature is monitored with thermocouples embedded in the microchannel inlets and outlets. (b), (c) Top and side view of the simulation model (dimensions in mm). The microvascular composite panel is heated from below while coolant circulates through all channels at a set inlet temperature and flow rate.

Model F32-HP) at 21 °C and pumped through the composite with a peristaltic pump (Cole-Parmer Masterflex, Model EW-07551099). Coolant flow was evenly divided between channels. Tubing lines were connected to the composite with 19 gauge needle fittings. The fittings contained Type T thermocouple probes (Omega, part # TMQSS-020U-36) to measure coolant temperature, which were inserted by drilling a hole into the fittings and sealing the thermocouple with acrylate adhesive (Loctite Depend 330). For 3, 4, and 6-channel panels, thermocouples were placed at all channel inlets and outlets. For 8 and 12-channel panels, thermocouples were placed at every other inlet and outlet. Thermocouple measurements were taken using 4-port thermocouple readers (Phidgets Inc., model 1048) controlled using LabVIEW 2013. Surface temperature measurements of the panel were taken with an infrared camera (FLIR, Model SC620).

Experiments were performed to measure the surface temperature and the average coolant temperature rise (ΔT_c) at steady-state. The cooling efficiency (η) of the panel was then calculated as the ratio of the heat flux absorbed by the channels (q_c) to the total heat flux applied (q_t) using equation (1):

$$\eta = \frac{q_c}{q_t}, \quad (1)$$

where $q_c = \dot{m}c_p \Delta T_c$, \dot{m} is total coolant flow rate, and c_p is the specific heat of the coolant.

2.3. Model conditions for CFD simulations

The cooling performance of microvascular panels was analyzed using the commercial CFD package ANSYS Fluent v15.0. The model simulated is shown in figures 3(b) and (c) and consists of a vascular composite heated from one side (copper plate/heater) and open to convection and radiation on the opposite side. The side walls are insulated in the plane and coolant is circulated with a constant inlet temperature (21.5 °C) based on the average inlet temperature read by thermocouples during experiments.

The full set of dimensions, boundary conditions, and material properties used for simulations is included in table 1.

A surface convection coefficient of $h = 8 \text{ W m}^{-2} \text{ K}^{-1}$ was chosen after fitting to experimental data. The emissivity of the top surface was set to 0.97 to represent the matte black painted surface. Coolant material properties were taken from literature [33] and composite properties were calculated based on constituent properties and fiber volume fraction (see table 1).

A set of simulations was also performed to analyze cooling performance under conditions more realistic for *in situ* battery packaging. In this case, panels are heated from both top and bottom surfaces (see figure 1(b)), there is no copper plate between the panels and the batteries, and the coolant inlet temperature would likely be higher than room temperature [33]. Commercial microvascular panels would also maximize fiber volume fraction and thus, thermal conductivity (see table 1). Simulations for these conditions were also performed for aluminum panels as a comparison case.

2.4. Mesh generation and convergence

Conforming, hexahedral finite volume meshes of microvascular panels were constructed in ANSYS Meshing v14.5. A mesh convergence study was performed on a panel 3 mm thick with 6 embedded microchannels. Figure S2 shows a convergence plot of average surface temperature for the panel versus the number of fluid elements in the mesh. Based on this study, a maximum fluid mesh sizing of 40 μm was defined yielding 350 000 fluid elements and 750 000 total elements for the 6-channel panel. The same mesh sizings were used for all other panels, yielding a range of 410 000–4000 000 total elements for all panels simulated.

Simulations were performed in ANSYS Fluent using the SIMPLE pressure–velocity coupling scheme, Green-Gauss node-based gradient discretization, second-order pressure discretization, third-order MUSCL momentum discretization, and third-order MUSCL energy discretization. The simulations

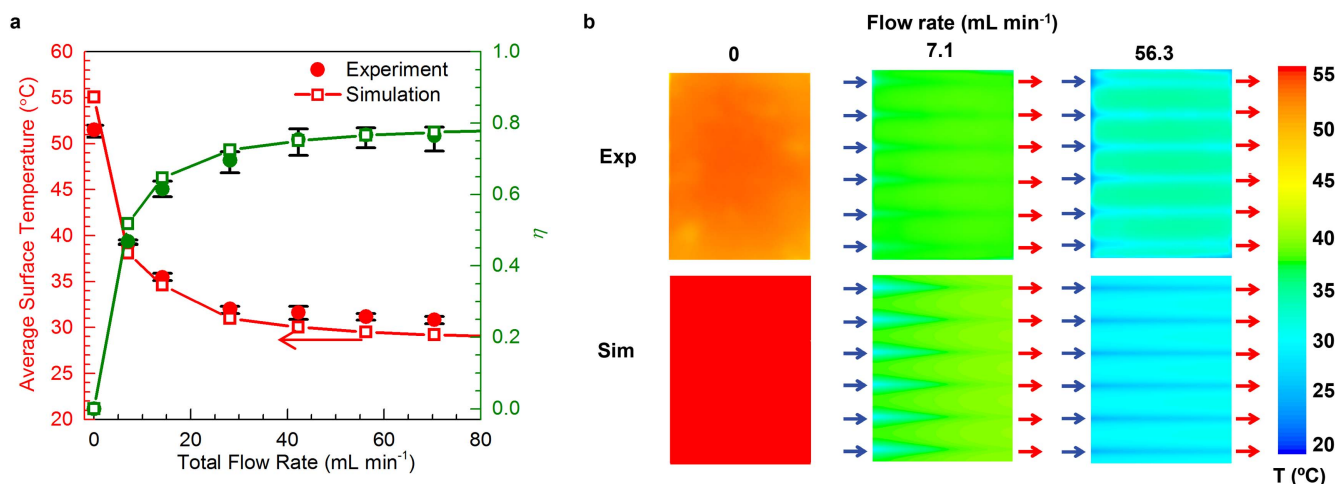


Figure 4. Thermal performance of a 6-channel PAN-based carbon/epoxy panel subject to 500 W m^{-2} applied heat flux as a function of total coolant flow rate. (a) Plot of average steady-state surface temperature and cooling efficiency (η) versus flow rate. Error bars represent the maximum and minimum values for 3 samples. (b) Representative surface temperature profiles for experiment and simulation at different flow rates.

solve for the conservation of mass, momentum, and energy across a finite volume mesh for a Newtonian, incompressible fluid with laminar flow. The maximum Reynolds number for any simulation was ca. 200, confirming the assumption of laminar flow. Simulations were performed to obtain the temperature profile of the panels at steady-state. The convergence criterion employed was for velocity and continuity residuals to reach 10^{-4} and for the energy residual to reach 10^{-9} . These thresholds were sufficient for full convergence of panel and coolant temperature fields.

3. Results and discussion

3.1. Experimental characterization of cooling performance

3.1.1. Effect of coolant flow rate. A parametric study was performed to characterize cooling panels across a wide range of operating conditions. The baseline test case consists of a 500 W m^{-2} applied heat flux and 28.2 mL min^{-1} (0.5 g s^{-1}) total flow rate applied to a 6-channel PAN-based carbon/epoxy vascular panel. The heater size and baseline heat flux are representative of the thermal load of one battery cell in the Chevrolet Volt [33, 34]. These tests represent a 1:1 battery cell: cooling panel ratio as shown for the stacking sequence in figure 1(b). The choice of coolant and baseline flow rate are also inspired by the Chevrolet Volt system [33, 34].

The effect of total flow rate on the cooling performance of a 6-channel PAN-based carbon/epoxy panel is shown in figure 4. Three panels were tested for repeatability: two panels in which channels were made with nylon monofilament and one panel where the channels were made with the VaSC technique. No significant difference was seen between panels made with the different fabrication techniques. For the case where no flow occurs, the average panel surface temperature is $\sim 52^\circ\text{C}$ and all heat is lost through radiation and convection to the environment. As the flow rate is increased, heat is absorbed by the coolant and transported through the channels. Average panel temperature quickly decreases until reaching a

plateau value at high flow rate, as does the maximum surface temperature (see summary of all experimental data in table 2). Surface temperature profiles reveal warm regions between channels and a slight increase in temperature in the direction of coolant flow.

Cooling efficiency (η) quickly increases with increasing flow rate (figure 4) until reaching about 80% at high flow rates. Flow rates above $30\text{--}40 \text{ mL min}^{-1}$ are observed to provide minimal additional cooling capability while requiring higher pump pressure and power. Good agreement was obtained between experimental data and simulation results for surface temperature and cooling efficiency across all conditions tested. Small discrepancies between experimental and simulated values are likely experimental error and/or variation in convection coefficient (see discussion in section S3).

3.1.2. Effect of heat flux. The effect of applied heat flux on cooling performance for a 6-channel PAN-based carbon/epoxy panel is presented in figure 5. Higher heat fluxes represent higher power density batteries and more rapid charge/discharge conditions. Average and maximum surface temperature (and ΔT_c) rise linearly with heat flux as expected. Cooling efficiency is roughly constant over the range of heat fluxes tested.

3.1.3. Effect of channel spacing. Composite panels with 3, 4, 6, 8, and 12 channels were tested to study the effect of channel spacing on cooling performance. The results of this study (figure 6) reveal that average surface temperature decreases and cooling efficiency increases with increasing number of channels. The better cooling performance is due to both an increase in channel surface area, which results in lower radial thermal gradients within channels [35], and by the reduction in distance between channels (and the resulting reduction in heat conduction distance to channels).

3.1.4. Effect of fiber conductivity. While PAN-based carbon fibers are the most common and economical class of carbon

Table 1. Dimensions, boundary conditions, and material properties used for cooling simulations.

Simulation condition/material property	Value for experimental validation	Value for <i>in situ</i> battery cooling	Reference
Panel dimensions			
Panel width (mm)	150	160	
Panel height (mm)	200	200	
Panel thickness (mm)	2.7 ^a	3 ^b	
Channel diameter (mm)	0.5	0.5	
Channel location through-thickness	Centered	Centered	
Channel spacing	See table S1	See table S1	
Boundary conditions			
Applied heat flux (W m^{-2})	500 from back ^b	250 from front and 250 from back ^b	
Total coolant flow rate (ml min^{-1})	28.2 ^b	28.2 ^b	
Coolant inlet temperature ($^{\circ}\text{C}$)	21.5	27	
Coolant outlet pressure (Pa)	0	0	
Thickness of copper plate between heater and composite (mm)	1.6	N/A	
Convection coefficient h for top face ($\text{W m}^{-2} \text{K}^{-1}$)	8	N/A	
Emissivity for top face	0.97	N/A	
Air temperature ($^{\circ}\text{C}$)	21	N/A	
Sides of panel	Insulated	Insulated	
Coolant: 50/50 water/ethylene glycol			
Density (kg m^{-3})	1065	1065	[33]
Viscosity (Pa s)	$0.0069*(T/273)^{-8.3}$	$0.0069*(T/273)^{-8.3}$	[33]
Specific heat ($\text{J kg}^{-1} \text{K}^{-1}$)	$2574.7 + 3.0655 T$	$2574.7 + 3.0655 T$	[33]
Thermal conductivity ($\text{W m}^{-1} \text{K}^{-1}$)	0.419	0.419	[33]
PAN-based carbon fiber composite			
Fiber volume fraction V_f (%)	49.5	60	ASTM D3171
Density (kg m^{-3})	1440	1500	^c
Specific heat ($\text{J kg}^{-1} \text{K}^{-1}$)	880	860	^c
In-plane thermal conductivity ($\text{W m}^{-1} \text{K}^{-1}$)	2.2	2.7	^c
Transverse thermal conductivity ($\text{W m}^{-1} \text{K}^{-1}$)	0.47	0.59	^c
Pitch-based carbon fiber composite			
Fiber volume fraction (%)	38.3	60	ASTM D3171
Density (kg m^{-3})	1490	1710	^c
Specific heat ($\text{J kg}^{-1} \text{K}^{-1}$)	850	790	^c
In-plane thermal conductivity ($\text{W m}^{-1} \text{K}^{-1}$)	48	75	^c
Transverse thermal conductivity ($\text{W m}^{-1} \text{K}^{-1}$)	0.39	0.61	^c
Aluminum			
Density (kg m^{-3})	N/A	2720	Fluent 15.0
Specific heat ($\text{J kg}^{-1} \text{K}^{-1}$)	N/A	870	Fluent 15.0
Thermal conductivity ($\text{W m}^{-1} \text{K}^{-1}$)	N/A	202	Fluent 15.0

^a Value of 3 mm used for pitch-based carbon fiber composite.

^b Baseline value. Other values were also tested.

^c Determined using constituent properties and fiber volume fraction. Epoxy properties and fiber properties are given in table S2. Density and specific heat were determined by rule of mixtures. Conductivity was determined using the rule of mixtures for axial conductivity and the self-consistent model for transverse conductivity (see [19] for calculations).

fiber, pitch-based carbon fibers offer substantially higher axial thermal conductivity (ca. $250 \text{ W m}^{-1} \text{K}^{-1}$ for pitch-based carbon fiber versus ca. $8 \text{ W m}^{-1} \text{K}^{-1}$ for PAN-based carbon fiber). A 3-channel pitch-based carbon/epoxy panel was fabricated and tested to compare to an equivalent PAN-based

carbon/epoxy panel. The pitch-based panel produces a much more uniform temperature distribution compared to the PAN-based panel (figure 7). The higher in-plane thermal conductivity reduces in-plane thermal gradients, lowering the average surface temperature and increasing cooling efficiency.

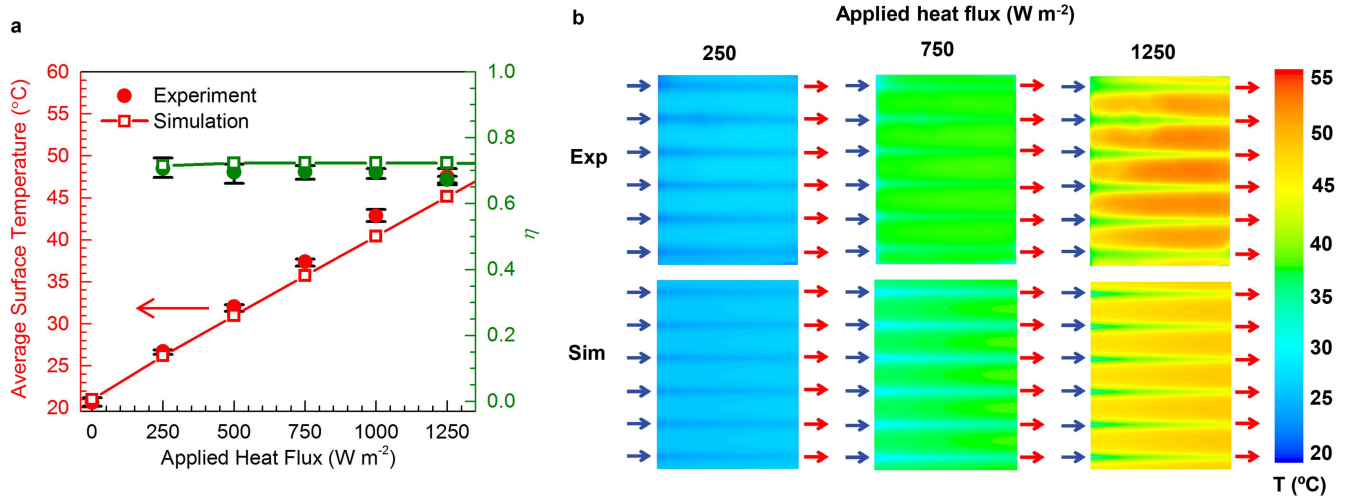


Figure 5. Thermal performance of a 6-channel PAN-based carbon/epoxy panel subject to 28.2 mL min⁻¹ total flow rate as a function of applied heat flux. (a) Plot of average steady-state surface temperature and cooling efficiency (η) versus applied heat flux. Error bars represent the maximum and minimum values for 3 samples. (b) Representative surface temperature profiles for experiment and simulation at different applied heat fluxes.

Table 2. Comparison of average steady-state surface temperature T_{av} , maximum surface temperature T_{max} , and coolant temperature rise ΔT_c for experiments and simulations. Experimental error refers to the largest deviation of any sample from the mean value. The baseline test conditions are in bold.

Sample	Samples tested	Heat flux (W m ⁻²)	Total flow rate (mL min ⁻¹)	T_{av} (°C)		T_{max} (°C)		ΔT_c (°C)	
				Sim.	Exp.	Sim.	Exp.	Sim.	Exp.
6-channel PAN	3	500	0	55.1	51.5 ± 0.8	55.1	52.6 ± 0.4	N/A	N/A
	“	“	7.1	38.1	39.1 ± 0.1	39.5	40.8 ± 0.2	17.7	16.1 ± 0.2
	“	“	14.1	34.6	35.5 ± 0.4	35.0	37.2 ± 0.6	11.1	10.6 ± 0.4
	“	“	28.2	31.0	32.0 ± 0.5	32.3	33.6 ± 0.5	6.2	6.0 ± 0.3
	“	“	42.3	30.0	31.6 ± 0.7	31.3	33.2 ± 0.8	4.3	4.3 ± 0.3
	“	“	56.4	29.5	31.2 ± 0.4	30.7	32.8 ± 0.4	3.3	3.3 ± 0.2
6-channel PAN	3	250	28.2	26.4	26.7 ± 0.3	26.8	27.7 ± 0.3	3.1	3.0 ± 0.1
	“	750	“	36.9	37.4 ± 0.5	37.7	39.7 ± 0.6	9.3	9.0 ± 0.3
	“	1000	“	42.2	42.9 ± 0.7	43.0	45.9 ± 0.8	12.4	11.9 ± 0.3
	“	1250	“	46.8	47.5 ± 1.0	48.3	51.1 ± 0.8	15.5	14.4 ± 0.3
3-channel PAN	1	500	28.2	35.1	36.7	36.2	38.4	5.2	5.0
4-channel PAN	“	“	“	33.2	34.8	34.4	36.5	5.7	5.7
8-channel PAN	“	“	“	29.7	31.0	31.0	32.7	6.5	7.1
12-channel PAN	“	“	“	28.3	30.1	29.6	31.5	6.9	7.3
3-channel Pitch	“	“	“	30.0	32.5	31.2	33.5	6.4	6.4

Pitch-based carbon fiber composites offer superior cooling performance compared to PAN-based carbon fiber composites, albeit at higher material cost.

3.2. Simulations of *in situ* battery cooling

3.2.1. Effect of panel material and channel spacing. The Fluent model was validated by experiments across a wide range of operating conditions. Further simulations were also performed that better represent *in situ* battery pack cooling

conditions. These simulations consist of a vascular carbon/epoxy composite panel being heated from both top and bottom surfaces. Composite panels were assumed to have a higher fiber volume fraction of 60% and the coolant inlet temperature was increased to 27 °C. The cooling performance objective for these simulations is to maintain a steady-state temperature below 40 °C.

Three panel materials with different thermal conductivities were simulated: PAN-based carbon/epoxy ($k = 2.7 \text{ W m}^{-1} \text{ K}^{-1}$ in-plane), pitch-based carbon/epoxy ($k = 75 \text{ W m}^{-1}$

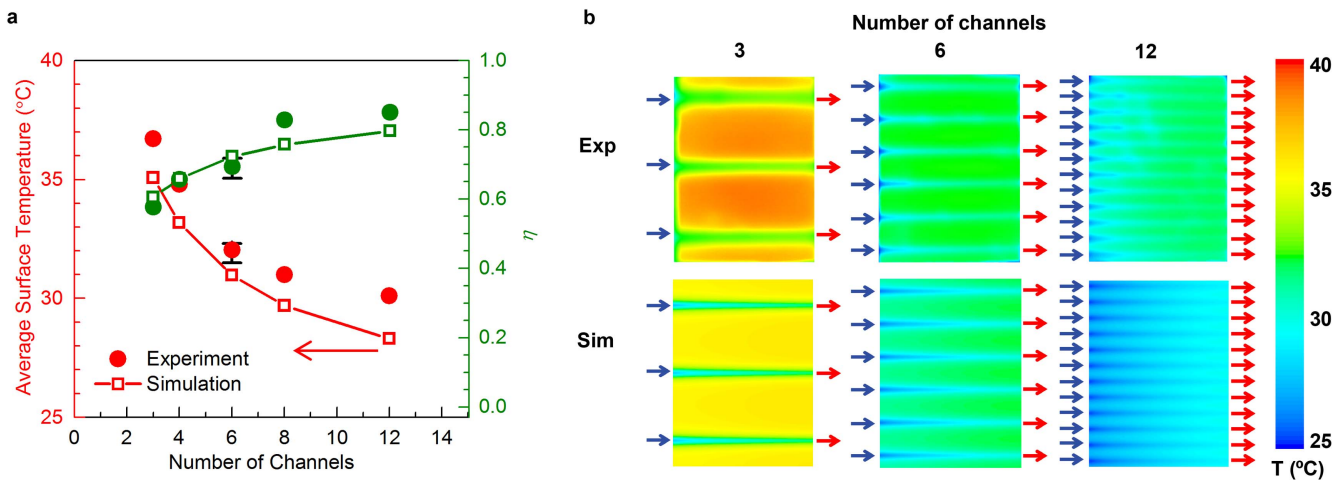


Figure 6. Thermal performance of PAN-based carbon/epoxy panels with 3, 4, 6, 8, and 12 channels at 500 W m^{-2} applied heat flux and 28.2 mL min^{-1} total coolant flow rate. (a) Plot of average steady-state surface temperature and cooling efficiency (η) versus number of channels. The error bars represent the maximum and minimum values for 3 samples for the 6-channel sample. (b) Surface temperature profiles for experiment and simulation for panels with different numbers of channels.

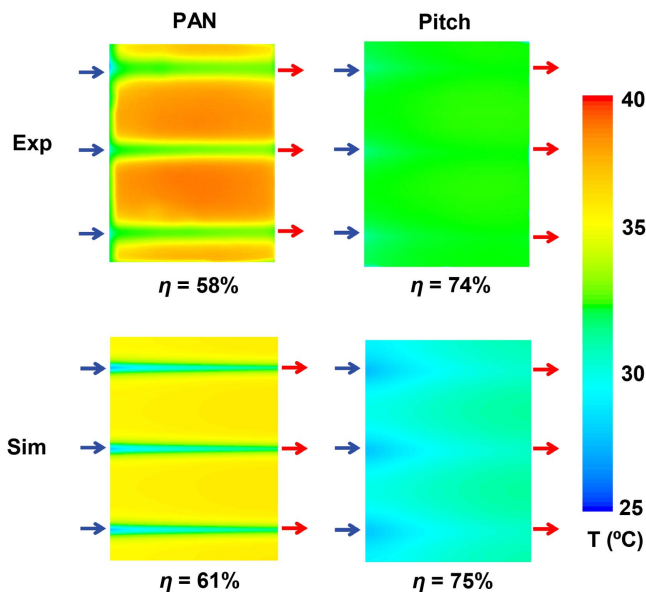


Figure 7. Comparison of steady-state surface temperature profiles for 3-channel panels made with PAN-based carbon/epoxy and pitch-based carbon/epoxy. The applied heat flux was 500 W m^{-2} and the total coolant flow rate was 28.2 mL min^{-1} . Cooling efficiency η is noted for each case.

K^{-1}), and aluminum ($k = 202 \text{ W m}^{-1} \text{ K}^{-1}$) as a reference case. Panels with these materials and different numbers of channels were simulated for a total applied heat flux of 500 W m^{-2} and a total coolant flow rate of 28.2 mL min^{-1} (figure 8). Aluminum panels performed well and satisfied the target temperature requirement in all cases. Pitch-based carbon/epoxy panels also performed well and met the target temperature requirement for all cases greater than 4 cooling channels.

PAN-based carbon/epoxy panels with a small number of cooling channels reach temperatures far above the target value due to hot spots forming between channels (figure 8(b)). As the number of cooling channels increases, the temperature

distribution becomes more uniform and the maximum temperature drops significantly. The 16-channel PAN-based carbon/epoxy panel has a maximum temperature below the target value and a temperature profile similar to panels made with pitch-based carbon/epoxy and aluminum. The lower thermal conductivity of PAN-based carbon/epoxy can thus be offset by increasing channel density. Meanwhile, PAN-based carbon/epoxy panels provide significantly higher specific strength, stiffness, and crashworthiness than aluminum panels [16].

The incorporation of a high volume fraction of microchannels can potentially reduce the mechanical properties of a composite [36–39]. However, the 16-channel panel has a channel spacing of 13 mm and a channel volume fraction of only 0.5%. Pety *et al* recently confirmed that microchannels can be incorporated into a carbon/epoxy composite at this spacing without reducing crashworthiness [29]. Crush tests on microvascular panels revealed no loss in SEA for channels both aligned and misaligned with the loading direction. In addition, Coppola *et al* demonstrated that microchannels can be integrated into a woven composite at this volume fraction without reducing strength or stiffness [40].

3.2.2. Effect of coolant flow rate and heat flux. The performance of a 16-channel PAN-based carbon/epoxy panel was further analyzed at different applied heat fluxes and flow rates (figure 9(a)). For a given heat flux, maximum surface temperature drops quickly with increasing flow rate at first and then begins to plateau. For a given flow rate, increasing heat flux gives linearly increasing surface temperatures, as expected. Interestingly, the panel can cool to the temperature target even at double the baseline heat flux (1000 W m^{-2} total) if a high enough flow rate is used ($>80 \text{ mL min}^{-1}$).

Pumping pressure for the 16-channel panel is plotted versus flow rate in figure 9(b). Pressure rises linearly as expected. The

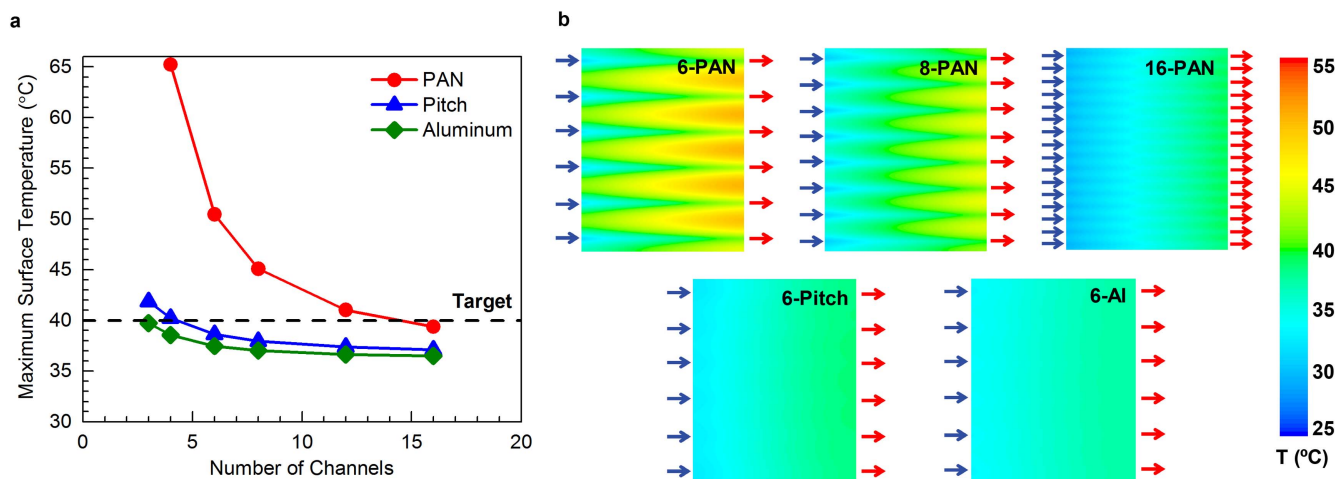


Figure 8. Simulation results for *in situ* battery cooling using 3 mm thick panels with different materials and channel spacing. (a) Maximum steady-state surface temperature versus number of channels for panels made with PAN-based carbon/epoxy, pitch-based carbon/epoxy, and aluminum. A heat flux of 250 W m^{-2} is applied from both sides and the total coolant flow rate is 28.2 mL min^{-1} . (b) Surface temperature contours for various panels.

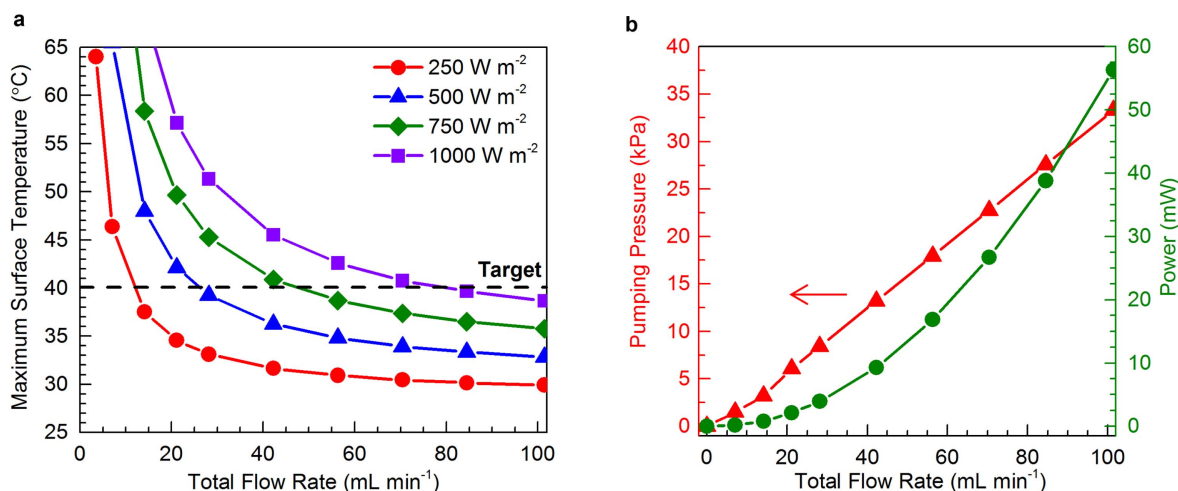


Figure 9. Simulation results for *in situ* battery cooling using a 16-channel PAN-based carbon/epoxy panel. (a) Maximum steady-state surface temperature for a 3 mm thick panel subject to various total applied heat flux and total coolant flow rate. (b) Average pumping pressure and power versus flow rate. Results are shown for a total applied heat flux of 500 W m^{-2} .

maximum pressure (33 kPa) is well within the range of commercial automotive coolant pumps, which operate at pressures up to ca. 120 kPa [41]. Pumping power was also calculated by multiplying pressure by volumetric flow rate (figure 9(b)). Power increases with the square of flow rate as expected. The maximum power is only 56 mW, which is less than 0.001% of the ca. 10 kW of power available from a typical EV battery during operation [2].

3.2.3. Effect of panel thickness. Simulations were also performed on 16-channel panels with thicknesses ranging from 1–5 mm. Channels were centered across the cross-section for all panels. Panel thickness had no significant impact on surface temperature (figure 10) since the panels are all thin enough to prevent large transverse thermal gradients. Thus, without

sacrificing cooling performance, thin panels can be used to reduce weight while thicker panels can be used to provide increased mechanical protection.

4. Conclusions

Microvascular carbon/epoxy composites were explored as novel materials for battery packaging. Cooling experiments on PAN-based carbon/epoxy vascular panels showed exceptional performance at high total coolant flow rate ($>20 \text{ mL min}^{-1}$) and channel density. Cooling performance was further improved for pitch-based carbon/epoxy panels due to their higher in-plane thermal conductivity ($k \approx 50 \text{ W m}^{-1} \text{ K}^{-1}$ versus $2 \text{ W m}^{-1} \text{ K}^{-1}$ for PAN-based carbon/epoxy). CFD simulations using Fluent

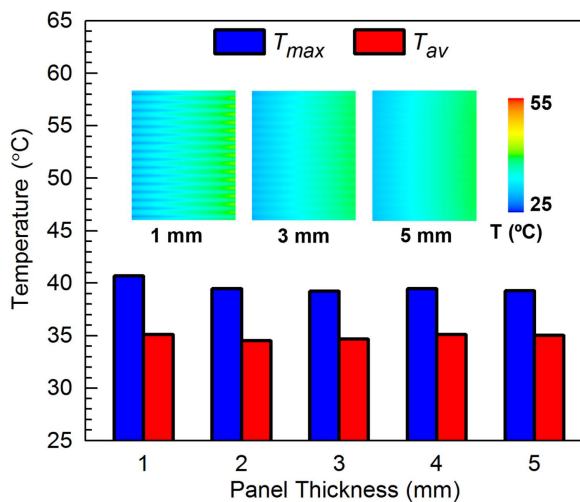


Figure 10. Effect of thickness on the average and maximum surface temperature of panels subject to *in situ* battery cooling conditions. Simulations were performed with an applied heat flux of 500 W m^{-2} and a total flow rate of 28.2 mL min^{-1} . Insets show surface temperature profiles for the 1, 3, and 5 mm thick panels.

were validated across a wide range of testing conditions by experimental data.

Further simulations confirmed that both pitch-based and PAN-based carbon/epoxy panels with sufficient channel density can satisfactorily cool EV battery packs of the Chevrolet Volt class. The required number of $500 \mu\text{m}$ cooling channels in a 200 mm long panel is 4 for pitch-based carbon/epoxy and 16 for PAN-based carbon/epoxy.

This study was the first to demonstrate that microvascular composites can serve as cooling panels to keep a heat source within a desired temperature range. The thoroughly validated CFD solver can now be used to optimize composites for other applications requiring active cooling and structural protection. Work is ongoing to develop composite cooling panels for fuel cells, microelectronics, antennas [42], and satellites [43]. Work is also ongoing to design battery cooling panels with more advanced 2D channel networks [44].

Acknowledgments

This work was supported by the Air Force Office of Scientific Research (Grant No. FA9550-15-1-0087) and the Center for Electrical Energy Storage, an Energy Frontier Research Center funded by the U.S. DOE, Office of Basic Energy Sciences. SJP was supported by DoD, AFOSR, National Defense Science and Engineering Graduate (NDSEG) Fellowship, 32 CFR 168a. The authors extend gratitude to Prof. Nancy Sottos for helpful discussion; Kevin Hart, Tony Coppola, Jason Patrick, and Piyush Thakre for composite manufacture and testing; Travis Ross of the Beckman Visualization Laboratory for help with ANSYS Fluent; Philip Barnett for help with figure preparation; and Cytec for the donation of carbon fiber fabric.

References

- [1] Bandhauer T M, Garimella S and Fuller T F 2011 A critical review of thermal issues in lithium-ion batteries *J. Electrochem. Soc.* **158** R1
- [2] Neubauer J and Wood E 2014 Thru-life impacts of driver aggression, climate, cabin thermal management, and battery thermal management on battery electric vehicle utility *J. Power Sources* **259** 262–75
- [3] Schuster E, Ziebert C, Melcher A, Rohde M and Seifert H J 2015 Thermal behavior and electrochemical heat generation in a commercial 40 Ah lithium ion pouch cell *J. Power Sources* **286** 580–9
- [4] Lindgren J and Lund P D 2016 Effect of extreme temperatures on battery charging and performance of electric vehicles *J. Power Sources* **328** 37–45
- [5] Finegan D P *et al* 2015 In-operando high-speed tomography of lithium-ion batteries during thermal runaway *Nat. Commun.* **6** 6924
- [6] He F, Li X and Ma L 2014 Combined experimental and numerical study of thermal management of battery module consisting of multiple Li-ion cells *Int. J. Heat Mass Transf.* **72** 622–9
- [7] Jayaraman S, Anderson G, Kaushik S and Klaus P 2011 Modeling of battery pack thermal system for a plug-in hybrid electric vehicle *SAE Tech. Rep.* 2011-01-0666
- [8] Hamut H S, Dincer I and Naterer G F 2014 Experimental and theoretical efficiency investigation of hybrid electric vehicle battery thermal management systems *J. Energy Resour. Technol.* **136** 11202
- [9] Giuliano M R, Advani S G and Prasad A K 2011 Thermal analysis and management of lithium–titanate batteries *J. Power Sources* **196** 6517–24
- [10] Tran T-H, Harmand S, Desmet B and Filangi S 2014 Experimental investigation on the feasibility of heat pipe cooling for HEV/EV lithium-ion battery *Appl. Therm. Eng.* **63** 551–8
- [11] Kizilel R, Lateef A, Sabbah R, Farid M M, Selman J R and Al-Hallaj S 2008 Passive control of temperature excursion and uniformity in high-energy Li-ion battery packs at high current and ambient temperature *J. Power Sources* **183** 370–5
- [12] Smith B 2012 Chevrolet volt battery incident overview report *Technical Report DOT-HS 811573* <http://odi.nhtsa.gov/acms/cs/jaxrs/download/doc/UCM399393/INRP-PE11037-49880.pdf>
- [13] Aylor A 2012 Chevrolet Volt battery pack tests *Technical Report GTL-DOT-11-VOLTBAT 2012* http://jensenhughes.com/wp-content/uploads/2014/02/White_Paper_Chevy-Volt-Battery-Pack-Tests_USDOT-NHTSA_AAylor-GBack-CWinchester_JAN-2012.pdf
- [14] Grauers L, Olsson R and Gutkin R 2014 Energy absorption and damage mechanisms in progressive crushing of corrugated NCF laminates: fractographic analysis *Compos. Struct.* **110** 110–7
- [15] Barnes G, Coles I, Roberts R, Adams D O and Garner D M 2010 Crash safety assurance strategies for future plastic and composite intensive vehicles *Report Number DOT-VNTSC-NHTSA-10-01* (<https://nhtsa.gov/DOT/NHTSA/NVS/Crashworthiness/Plastics/DOT-VNTSC-NHTSA-10-01.pdf>)
- [16] Lukaszewicz D H-J A 2014 Automotive composite structures for crashworthiness *Advanced Composite Materials for Automotive Applications: Structural Integrity and Crashworthiness* ed A Elmarakbi (Chichester: Wiley) pp 99–127
- [17] Phillips D M, Ryan Pierce M and Baur J W 2011 Mechanical and thermal analysis of microvascular networks in structural composite panels *Composites A* **42** 1609–19
- [18] Soghrati S, Najafi A R, Lin J H, Hughes K M, White S R, Sottos N R and Geubelle P H 2013 Computational analysis

- of actively-cooled 3D woven microvascular composites using a stabilized interface-enriched generalized finite element method *Int. J. Heat Mass Transf.* **65** 153–64
- [19] Coppola A M, Griffin A S, Sottos N R and White S R 2015 Retention of mechanical performance of polymer matrix composites above the glass transition temperature by vascular cooling *Composites A* **78** 412–23
- [20] McElroy M W, Lawrie A and Bond I P 2015 Optimisation of an air film cooled CFRP panel with an embedded vascular network *Int. J. Heat Mass Transf.* **88** 284–96
- [21] Coppola A M, Warpinski L G, Murray S P, Sottos N R and White S R 2016 Survival of actively cooled microvascular polymer matrix composites under sustained thermomechanical loading *Composites A* **82** 170–9
- [22] Coppola A M, Hu L, Thakre P R, Radovic M, Karaman I, Sottos N R and White S R 2016 Active cooling of a microvascular shape memory alloy-polymer matrix composite hybrid material *Adv. Eng. Mater.* **18** 1145–53
- [23] Yu K, Phillips D M, Baur J W and Qi H J 2015 Analysis of shape-memory polymer composites with embedded microvascular system for fast thermal response *J. Compos. Mater.* **49** 1881–93
- [24] Li Y and Goulbourne N C 2015 Numerical simulations for microvascular shape memory polymer composites *Smart Mater. Struct.* **24** 55022
- [25] Asp L E and Greenhalgh E S 2014 Structural power composites *Compos. Sci. Technol.* **101** 41–61
- [26] Thomas J, Qidwai S, Pogue W and Pham G 2012 Multifunctional structure-battery composites for marine systems *J. Compos. Mater.* **47** 5–26
- [27] Belingardi G 2013 Energy absorbing sacrificial structures made of composite materials for vehicle crash design *Dynamic Failure of Composite and Sandwich Structures* ed S Abrate *et al* (New York: Springer) pp 577–610
- [28] Tan W and Falzon B G 2016 Modelling the crush behaviour of thermoplastic composites *Compos. Sci. Technol.* **134** 57–71
- [29] Pety S J, Sottos N R and White S R 2016 Crashworthiness of microvascular fiber-reinforced composites *Proc. American Society for Composites 31st Technical Conf.* pp 2422–9
- [30] Esser-Kahn A P, Thakre P R, Dong H, Patrick J F, Vlasko-Vlasov V K, Sottos N R, Moore J S and White S R 2011 Three-dimensional microvascular fiber-reinforced composites *Adv. Mater.* **23** 3654–8
- [31] Dong H, Esser-Kahn A P, Thakre P R, Patrick J F, Sottos N R, White S R and Moore J S 2012 Chemical treatment of poly (lactic acid) fibers to enhance the rate of thermal depolymerization *ACS Appl. Mater. Interfaces* **4** 503–9
- [32] Gergely R C R, Pety S J, Krull B P, Patrick J F, Doan T Q, Coppola A M, Thakre P R, Sottos N R, Moore J S and White S R 2015 Multidimensional vascularized polymers using degradable sacrificial templates *Adv. Funct. Mater.* **25** 1043–52
- [33] Jarrett A and Kim I Y 2011 Design optimization of electric vehicle battery cooling plates for thermal performance *J. Power Sources* **196** 10359–68
- [34] Jarrett A and Kim I Y 2014 Influence of operating conditions on the optimum design of electric vehicle battery cooling plates *J. Power Sources* **245** 644–55
- [35] Bergman T L, Lavine A S, Incropera F P and DeWitt D P 2007 *Fundamentals of Heat and Mass Transfer* (River Street, New Jersey: Wiley)
- [36] Norris C J, Bond I P and Trask R S 2011 The role of embedded bioinspired vasculature on damage formation in self-healing carbon fibre reinforced composites *Composites A* **42** 639–48
- [37] Hartl D J, Frank G J and Baur J W 2016 Effects of microchannels on the mechanical performance of multifunctional composite laminates with unidirectional laminae *Compos. Struct.* **143** 242–54
- [38] Kousourakis A and Mouritz A P 2010 The effect of self-healing hollow fibres on the mechanical properties of polymer composites *Smart Mater. Struct.* **19** 85021
- [39] Saeed M, Li B and Chen Z 2016 Mechanical effects of microchannels on fiber-reinforced composite structure *Compos. Struct.* **154** 129–41
- [40] Coppola A M, Thakre P R, Sottos N R and White S R 2014 Tensile properties and damage evolution in vascular 3D woven glass/epoxy composites *Composites A* **59** 9–17
- [41] Gilles T 2012 *Automotive Service: Inspection, Maintenance, Repair* (New York: Cengage Learning)
- [42] Hartl D J, Frank G J, Huff G H and Baur J W 2017 A liquid metal-based structurally embedded vascular antenna: I. Concept and multiphysical modeling *Smart Mater. Struct.* **26** 25002
- [43] Bunce D T, Bassett K P, Ghosh A R M, Barnett P R, Haken D M, Vrkljan S, Jagannatha R, Silva T and Coverstone V L 2016 Microvascular composite radiators for small spacecraft thermal management systems *Proc. 30th Annual AIAA/USU Conf. on Small Satellites* p SSC16-X-1
- [44] Tan M H Y, Najafi A R, Pety S J, White S R and Geubelle P H 2016 Gradient-based design of actively-cooled microvascular composite panels *Int. J. Heat Mass Transf.* **103** 594–606